HANDBOOK OF COMPOSITES

Series Editors: A. Kelly and Yu. N. Rabotnov

VOLUME 2

STRUCTURES AND DESIGN

Volume Editors: C. T. Herakovich and Y. M. Tarnopol'skii

North-Holland

Contents

CHAPTER 2

Mechanics of Unsymmetric Laminates

M.W. Hyer

Department of Engineering Science and Mechanics
Virginia Polytechnic Institute and State University
Blacksburg, VA 24061
U.S.A.

Contents

HANDBOOK OF COMPOSITES, VOL. 2 – Structure and Design
Edited by C.T. HERAKOVICH and Y.M. TARNOPOL'SKII

1. Introduction

Generally laminates are constructed so that for every lamina with specific material properties, thickness, fiber orientation, and location on one side of the laminate's geometric midplane, there is a lamina with identical material properties, thickness, and fiber orientation an equal distance on the other side of the midplane. Such laminates are referred to as symmetric laminates. Symmetric laminates are characterized by the fact that the bending–stretching stiffnesses, commonly denoted by the B_{ij} matrix, are zero. If a laminate is constructed so that symmetry about the midplane is not maintained, even for one pair of laminae, the laminate is referred to as an unsymmetric laminate. One or more entries in the B_{ij} matrix will be nonzero. Such a laminate will exhibit bending–stretching coupling under the influence of mechanical loads. In addition, such a laminate will exhibit rather unusual characteristics under the influence of thermal loads. This chapter addresses the latter topic. Specifically the chapter deals with the fact that unsymmetrically laminated resin–matrix composites which are flat at their elevated cure temperature do not remain flat when their temperature is lowered. This characteristic might be expected but it is not widely understood nor is it utilized. It is the purpose of this chapter to present the theory necessary for understanding the deformation characteristics of unsymmetric laminates as a function of temperature. Particular attention will be given to the out-of-plane deformations. The theory and numerical results discussed are limited to unsymmetric cross-ply laminates. Even with these simple laminates, the basic characteristics of the thermally-induced deformations can be understood and the effects of geometric and material properties studied. The work is presented to support the notion that shape, as well as stiffness and strength, can be tailored for a particular application of composites. The potential for shape-tailoring is quite important if it is realized that most structures, particularly aircraft structures, call for components with simple or compound curvatures. A flat structure is not as efficient as a shell structure and finds less usage. This chapter begins by describing in quite general terms the curing procedure for resin–matrix composites. A brief description of the curing process is necessary in order to illustrate the problem being addressed and provide insight into the mechanics involved. Examples of cured unsymmetric laminates are presented. Following that section the theory is outlined which can be used to predict the deformations of cross-ply unsymmetric laminates when their temperature is lowered from the cure temperature. The section after that presents a variety of numerical results to illustrate the influence of temperature, material properties, and laminate geometry.

2. Curing and the out-of-plane shapes of unsymmetric laminates

Flat elevated-temperature cure laminates are usually made by using a hot press or autoclave. In either case the laminate is made by laying the preimpregnated material, one layer at a time, on a flat steel plate, commonly called a caul plate. Release cloth, bleeder plys and other layers are associated with the fabrication process but for this discussion they are not important. After the desired number of layers are stacked, one on top of the other, another caul plate is secured on top of the layers. With this arrangement the precured laminate is sandwiched between the two steel plates. Often the whole assembly is vacuum bagged. The curing process then begins by increasing the temperature and pressure of the sandwiched layers. The elevated temperature and pressure are maintained for a period of time, according to the material manufacturer's specifications, and the resin begins to crosslink. After sufficient time has elapsed, the resin has fully cured and the temperature is decreased slowly to room temperature. The pressure is released and the laminate is ready for removal from the hot press or autoclave. If the laminate is symmetric, the cooled laminate, when removed from between the caul plates, is flat. Due to differences in the thermal expansion and elastic properties of the different laminae there can be significant residual stresses in the laminate. If the residual stresses are large enough, they can cause cracking. Other than cracks, there is little evidence of residual effects. On the other hand, if the laminate is unsymmetric, removal from the caul plates results in very obvious residual effects. Specifically, if the laminate is unsymmetric, it will not be flat when it is removed. Depending on the stacking sequence, there can be significant out-of-plane deformations. Deformations many times the laminate thickness are possible. Curiously enough, despite the wide range of unsymmetric laminates possible, the shape of the out-of-plane deformation has been observed to be either saddle-like or cylindrical. This was discussed by Hyer (1981a). The principal curvatures of the saddle or cylinder may or may not be aligned with the edges of the laminae. Fig. 1 shows a $(0_4/90_4)_T$ graphite–epoxy laminate at room temperature. As can be seen, the cooled laminate is cylindrical. When flat at its elevated cure temperature the laminate in Fig. 1 was approximately 150 mm × 150 mm. The laminate in Fig. 1 has its principal curvatures aligned with the edges of the laminate. Fig. 2 shows an example of a cylindrical laminate with the principal curvatures not aligned with the edges of the originally flat laminate. When flat this laminate was 100 mm × 100 mm. The laminate in Fig. 2 has a stacking arrangement of $(0/60/90_2)_T$ (not a cross-ply). Fig. 3 shows a 200 mm × 50 mm $(+45_2/-45_2)_T$ laminate. This laminate has twist curvature in the coordinate system aligned with the edges of the originally flat laminate.

In contrast to these examples, Fig. 4 shows the room-temperature shape of a $(0_{10}/90_{10})_T$ laminate. The dimensions of the laminate when it is flat are $150 \times 150\ mm^2$. From the figure it is obvious the laminate is saddle shaped. The laminates in Figs. 1–4 were all made from a material which cures at 177°C. It is important to note that the only difference between the laminate of Fig. 1 and

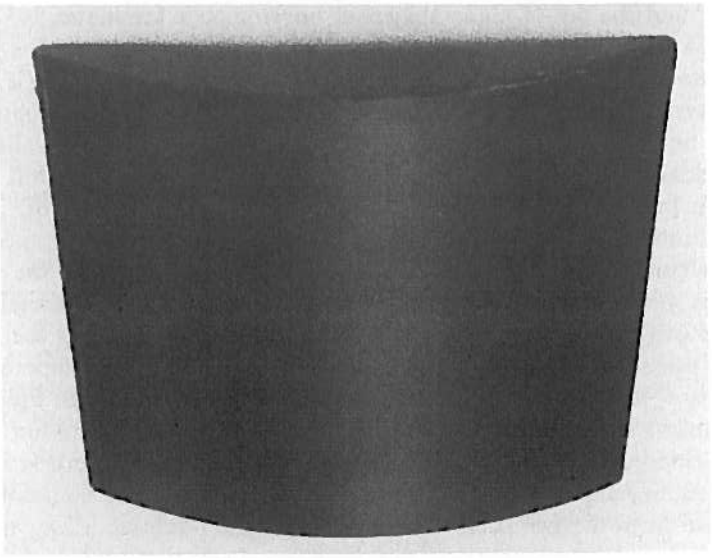

FIG. 1. The room-temperature shape of a 150 mm × 150 mm $(0_4/90_4)_T$ graphite–epoxy laminate.

the laminate of Fig. 4 is the thickness. It is obvious from these two figures that the shape observed at room temperature is dependent on the geometry of the laminate. This is a very important characteristic of unsymmetric laminates.

Another important characteristic of unsymmetric laminates is associated with the cylindrical shape. For some cylindrical laminates it is possible to force the cylindrical shape into another cylindrical shape. This is accomplished by a

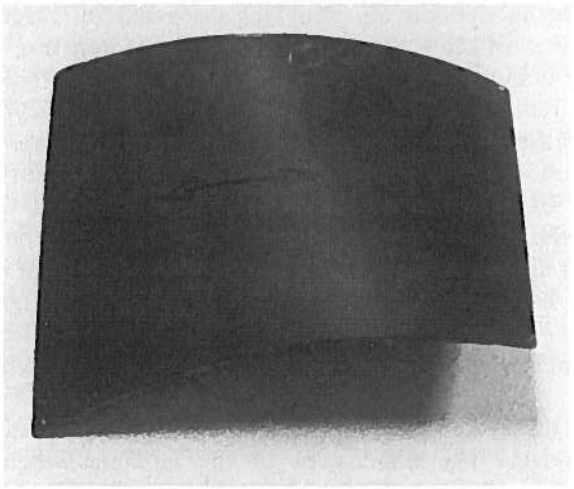

FIG. 2. The room-temperature shape of a 100 mm × 100 mm $(0/60/90_2)_T$ graphite–epoxy laminate.

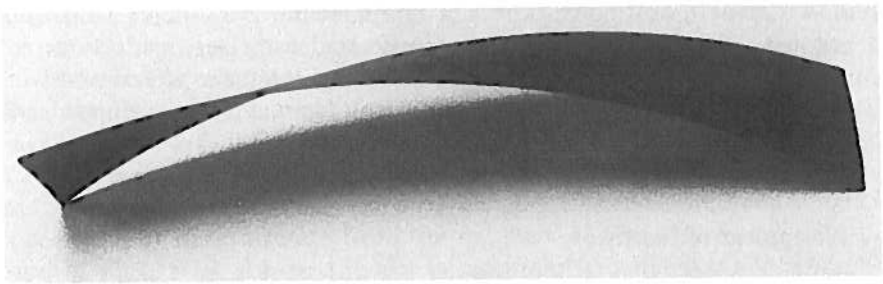

FIG. 3. The room temperature shape of a 200 mm × 50 mm $(+45_2/-45_2)_T$ graphite–epoxy laminate.

snap-through action. For other laminates, the cylindrical shape is unique, i.e., cannot be forced into another cylindrical shape. On the other hand, when the saddle shape appears, it is always unique. No other shape exists. As will be seen, it can be determined whether the shape is cylindrical or saddle, and whether the cylindrical shape is unique or whether it is possible for the unsymmetric laminate to have another cylindrical shape. In addition, it will be shown that while the laminate may have a cylindrical shape at room-temperature, it can be saddle shaped at a temperature closer to the cure temperature.

Figs. 1–4 show that there are unique characteristics associated with unsymmetric laminates. The behavior is not predicted by the method presented in the standard texts, for example, JONES (1975), AGARWAL and BROUTMAN (1980), TSAI and HAHN (1980). The method presented in the texts is usually referred to as classical lamination theory. The key to the behavior of unsymmetric laminates is the fact that the out-of-plane deflections associated with the shapes

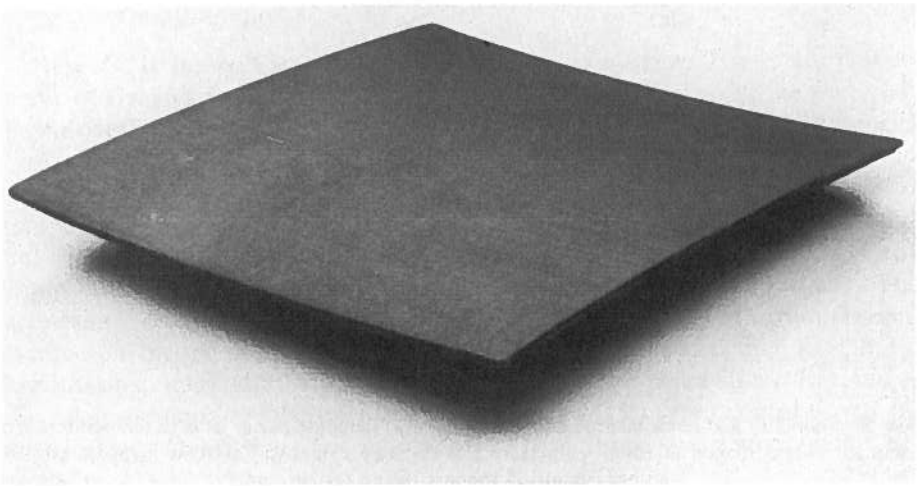

FIG. 4. The room-temperature shape of a 150 mm × 150 mm $(0_{10}/90_{10})_T$ graphite–epoxy laminate.

are many, many times the thickness of the laminate. Any theory which does not account for geometrically nonlinear effects due to large deflections is in error. A theory which accounts for geometrically nonlinear effects and which explains this unusual behavior of unsymmetric laminates is developed in the next section.

3. Development of the theory

Fig. 5 depicts schematically the problem being studied. Fig. 5(a) shows a laminate flat and undeformed at its elevated cure temperature. The figure also shows the x_1–x_2–x_3 reference coordinates system used throughout the analysis. The origin of the coordinates system is at the geometric center of the volume of the undeformed laminate. As stated in the introduction the study here will be limited to cross-ply laminates. This means that in Fig. 5(a) the layers in the laminate will have the fibers aligned either with the x_1-axis or with the x_2-axis. Figs. 5(b)–(d) show the room-temperature shapes discussed in the previous section. Fig. 5(b) shows a schematic of the saddle configuration. Figs. 5(c) and 5(d) show cylindrical shapes. These two cylindrical shapes can be thought to represent the two shapes related through snap-through for certain laminates.

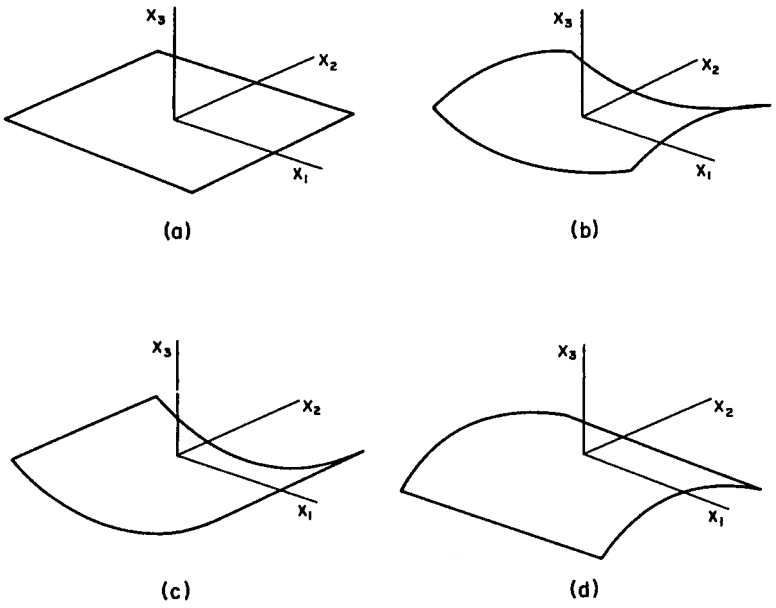

FIG. 5. Geometry and nomenclature of the problem: (a) laminate flat at its cure temperature; (b) laminate saddle shaped at room temperture; (c) laminate cylindrical at room temperature; (d) another cylindrical shape at room temperature.

On the other hand, one of the shapes can be thought to represent the unique cylindrical shape of other laminates. Since the laminates are cross-ply, the principal curvatures of the saddles or cylinders are aligned with the reference coordinate system. The laminate of Fig. 3 is cross-ply but not in a reference system aligned with the rectangular sides of the laminate. Such cases will not be considered here. The basic issue is to determine what fundamental mechanisms need to be included in an analysis of the thermo-mechanical cooling process so that the transition from the flat state of Fig. 5(a) to the deformed shape of Figs. 5(b), (c), or (d) can be accurately modeled. Of considerable importance is the fact that the geometric dimensions of a laminate have an influence on whether the flat laminate of Fig. 5(a) cools to the saddle shape given by 5(b) or whether it cools to the cylindrical shape given by Fig. 5(c). In addition, the snap-through to other cylindrical shape, Fig. 5(d), must be represented. Mathematically this latter point means multiple solutions to the governing equations (i.e. two equilibrium shapes at the same temperature). With multiple solutions the problem cannot be linear. It must be inherently nonlinear.

Here the theory governing the behavior of unsymmetric laminates will be developed from an energy viewpoint. The philosophy is simple: The shape (or shapes) observed for a given laminate at a given temperature is the shape that minimizes the total potential energy of the laminate. It will be assumed that the mechanical forces exerted on the laminate during the curing process do no net work on the laminate as the temperature changes from the cure temperature to room temperature. Thus the total potential energy to be considered is simply the strain energy in the cooled laminate.

The strain energy density, including the effects of thermal expansion, is given by

$$\omega = \tfrac{1}{2}\bar{C}_{ij}(e_i e_j - \alpha_i e_j \Delta T)\,, \quad i, j = 1\text{–}6\,. \tag{3.1}$$

Here $\bar{C}_{ij}$ is the stiffness matrix in the x_1–x_2–x_3 system. The e_i are components of Green's strain tensor in the x_1–x_2–x_3 system. The α_i are the material's linear coefficients of thermal expansion in the x_1–x_2–x_3 system. The temperature change is given by ΔT, ΔT positive corresponding to a temperature increase. Throughout the $\bar{C}_{ij}$ and α_i will be assumed to be independent of temperature. This is not a restriction on the analysis. Because of the large out-of-plane deformations associated with the temperature change, Green's strain tensor is used, as opposed to the strain tensor of linear elasticity. This assumption of the form of the strain tensor is the only deviation from classical lamination theory used in the present theory. It is assumed that Kirchhoff's hypothesis is valid and that each lamina is in a state of plane stress. Because of the latter assumption, the only components in eq. (3.1) that contribute to the strain energy density are e_1, e_2, and e_6. These three strain components are given by

$$e_1 = e_1^0 - x_3 \frac{\partial^2 u_3^0}{\partial x_1^2},$$

$$e_2 = e_2^0 - x_3 \frac{\partial^2 u_3^0}{\partial x_2^2}, \tag{3.2}$$

$$e_6 = e_6^0 - x_3 \frac{\partial^2 u_3^0}{\partial x_2 \partial x_1},$$

with

$$e_1^0 = \frac{\partial u_1^0}{\partial x_1} + \tfrac{1}{2}\left(\frac{\partial u_3^0}{\partial x_1}\right)^2,$$

$$e_2^0 = \frac{\partial u_2^0}{\partial x_2} + \tfrac{1}{2}\left(\frac{\partial u_3^0}{\partial x_2}\right)^2, \tag{3.3}$$

$$e_6^0 = \tfrac{1}{2}\left(\frac{\partial u_1^0}{\partial x_2} + \frac{\partial u_2^0}{\partial x_1} + \frac{\partial u_3^0}{\partial x_1}\frac{\partial u_3^0}{\partial x_2}\right).$$

The quantities e_i^0, $i = 1, 2, 6$, are the strains at the laminate midplane, u_1^0 is the displacement of a material point in the laminate in the x_1 direction, u_2^0 its displacement in the x_2 direction, and u_3^0 its displacement in the x_3 direction. The products of the strain gradients in eq. (3.3) represent the geometrically nonlinear effects due to large out-of-plane deformations (u_3^0).

Considering the plane stress state of the laminae and expanding eq. (3.1), the strain energy density becomes

$$\omega = \tfrac{1}{2}C_{11}' e_1^2 + C_{12}' e_1 e_2 + 2C_{66}' e_6^2 + \tfrac{1}{2}C_{22}' e_2^2 - (C_{11}'\alpha_1 + C_{12}'\alpha_2)e_1 \Delta T - (C_{12}'\alpha_1 + C_{22}'\alpha_2)e_2 \Delta T . \tag{3.4}$$

The C'-s are the reduced stiffnesses in the x_1–x_2–x_3 system. For cross-ply laminates C_{16}', C_{26}', and α_6 are zero.

Considering the entire laminate, the total potential energy is given by

$$W = \int_{x_1=-L_1/2}^{L_1/2} \int_{x_2=-L_2/2}^{L_2/2} \int_{x_3=-h/2}^{h/2} \omega \, dx_1 \, dx_2 \, dx_3 \tag{3.5}$$

The limits on the above volume integral reflect the fact that at the elevated cure temperature the flat laminate has length L_1 in the x_1 direction, L_2 in the x_2 direction and is of thickness h (in the x_3 direction). Recall that the origin of the coordinate system is located at the geometric center of the laminate.

To find the minimum value of total potential energy, eqs. (3.2) and (3.3) can be substituted into eq. (3.4) and those results substituted into eq. (3.5). Since the coordinate x_3 appears explicitly, integration with respect to x_3 will combine with the C'_{ij} to yield components of the extensional, coupling, and bending stiffnesses (A_{ij}, B_{ij}, and D_{ij}) of the laminate. In addition, integration with respect to x_3 results in effective thermal inplane forces, N_1^T and N_2^T, and moments, M_1^T and M_2^T. These effective thermal loads are given by

$$N_1^T = \Delta T \int_{-h/2}^{h/2} (C'_{11}\alpha_1 + C'_{12}\alpha_2)\, dx_3 , \tag{3.6a}$$

$$N_2^T = \Delta T \int_{-h/2}^{h/2} (C'_{12}\alpha_1 + C'_{22}\alpha_2)\, dx_3 , \tag{3.6b}$$

$$M_1^T = \Delta T \int_{-h/2}^{h/2} (C'_{11}\alpha_1 + C'_{12}\alpha_2)x_3\, dx_3 , \tag{3.6c}$$

$$M_2^T = \Delta T \int_{-h/2}^{h/2} (C'_{12}\alpha_1 + C'_{22}\alpha_2)x_3\, dx_3 . \tag{3.6d}$$

The expression for the total potential energy, W, will then be of the form

$$W = \int_{x_1=-L_1/2}^{L_1/2} \int_{x_2=-L_2/2}^{L_2/2} \omega(A_{ij}, B_{ij}, D_{ij}, N_1^T, N_2^T, M_1^T, M_2^T, u_1^0, u_2^0, u_3^0, x_1, x_2)\, dx_1\, dx_2 . \tag{3.7}$$

Seeking the stationary values of W with respect to variations in u_1^0, u_2^0, and u_3^0 leads to the differential equations and boundary conditions which govern the shape of the laminate at a given temperature. The equations will be nonlinear partial differential equations for u_1^0, u_2^0, and u_3^0 as functions of x_1 and x_2. These equations have not been derived. Except for selected cases it is felt that only approximate numerical solutions to the equations, e.g. finite-difference, finite-element, are possible. In addition, the first variation only provides information regarding equilibrium shapes. The equilibrium shapes may or may not exist in the laboratory. Since the problem is nonlinear, and since experimental observations indicated multiple shapes and a snap-through phenomenon, stability must be addressed. Obtaining solutions to the stability equations coupled with obtaining solutions to the equilibrium equations leads to a problem of significant proportions. The obtaining of numbers and conducting parameter studies becomes computer-intensive. Therefore, the approach here will be to seek approximate solutions in the sense of Ritz, starting with the energy expression

of eq. (3.7), and minimizing the expression in the context of simple assumed displacement fields. These displacement fields will be valid for the laminate as a whole.

From Figs. 1–4 it is clear an assumed out-of-plane displacement of the form

$$u_3^0(x_1, x_2) = \tfrac{1}{2}(ax_1^2 + bx_2^2)\,, \tag{3.8}$$

with a and b being unknown and to-be-determined constants, represents the possible shapes observed. With this functional form for u_3^0, $a = -b$ represents the saddle shape of Fig. 5(b), $a > 0$, $b = 0$ represents the cylindrical shape of Fig. 5(c) and $a = 0$, $b < 0$ represents the cylinder of Fig. 5(d). Functional forms to assume for $u_1^0(x_1, x_2)$ and $u_2^0(x_1, x_2)$ are not so obvious from Figs. 1–4. However, Fig. 6 provides some insight into the choice of functional form for these other two displacement fields. Fig. 6 shows a cross-section in the x_1–x_3 plane of a deformed laminate. It is not important whether the cross-section is

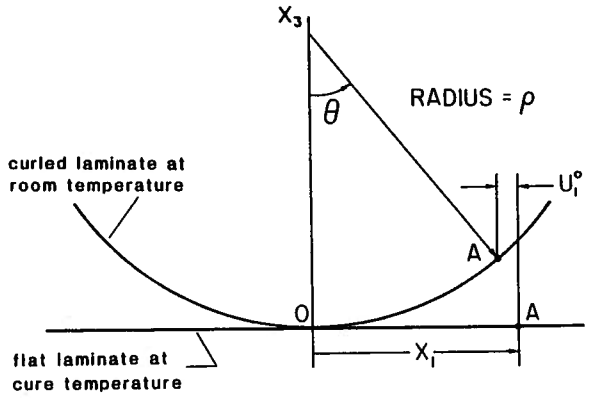

FIG. 6. Kinematics of a flat laminate deforming due to a temperature change.

associated with a cylinder or whether it is associated with a saddle. Shown in the figure is the cross-section when the laminate is flat and the cross-section when the laminate is at a lower temperature and curled out-of-plane. From the figure it is clear point A moves a significant amount in the negative x_1 direction due to the out-of-plane deformation. Specifically, point A moves an amount

$$u_1^0 = \rho \sin\theta - x_1\,, \tag{3.9}$$

x_1 being where point A was at the elevated cure temperature and ρ and θ geometric parameters indicated on Fig. 6. For small angular openings,

$$\sin\theta = \theta - \frac{\theta^3}{3!}\,. \tag{3.10}$$

If the inplane (arc-wise) strains are assumed small, the arc length from 0 to A is $\rho\theta$, or

$$\rho\theta = x_1 \tag{3.11}$$

Finally, from eq. (3.8),

$$1/\rho \cong a\,, \tag{3.12}$$

a being from eq. (3.8). Therefore, combining eqs. (3.9)–(3.12),

$$u_1^0 = -\tfrac{1}{6}a^2x_1^3\,. \tag{3.13}$$

Thermal effects, do however, contribute to the arc length 0A (Fig. 6) of the deformed laminate. As with classical lamination theory, it is assumed that the effect of thermal expansion (or contraction) in the x_1 direction is linear in x_1 and it superposes on the displacement due to curling, i.e.

$$u_1^0 = cx_1 - \tfrac{1}{6}a^2x_1^3\,, \tag{3.14}$$

c being an unknown constant.

Similar considerations in the x_2–x_3 plane lead to

$$u_2^0 = dx_2 - \tfrac{1}{6}b^2x_2^3\,, \tag{3.15}$$

d being a constant and b being from eq. (3.8). The quantities a, b, c and d will be determined as part of the minimization process.

Using eqs. (3.8), (3.14), and (3.15) in eq. (3.3) leads to

$$e_1^0 = c\,, \tag{3.16a}$$

$$e_2^0 = d\,, \tag{3.16b}$$

$$e_6^0 = abx_1x_2/2\,. \tag{3.16c}$$

For geometrically linear deformations of cross-ply laminates due to a temperature change, there are no midplane shearing strains, e_6^0. It can be reasoned that this is true for the large deformation geometrically nonlinear case. Eq. (3.16) contradicts this, i.e. $e_6^0 \neq 0$ in eq. (3.16), and so u_1^0 and u_2^0 of eqs. (3.14) and (3.15) must be modified to yield $e_6^0 = 0$. The final forms for u_1^0 and u_2^0 that do this are

$$\begin{aligned} u_1^0 &= cx_1 - \tfrac{1}{6}a^2x_1^3 - \tfrac{1}{4}abx_1x_2^2\,, \\ u_2^0 &= dx_2 - \tfrac{1}{6}b^2x_2^3 - \tfrac{1}{4}abx_2x_1^2\,. \end{aligned} \tag{3.17}$$

Eq. (3.17) along with eq. (3.8) form the assumed displacement fields for unsymmetric laminates deformed due to a temperature change relative to their cure temperature. These equations can be substituted into eqs. (3.2)–(3.4) and these in turn into eq. (3.5) and integration with respect to x_1 and x_2 performed in eq. (3.5). This substitution leads to an expression for W of the form

$$W = W(A_{ij}, B_{ij}, D_{ij}, N_1^T, N_2^T, M_1^T, M_2^T, L_1, L_2, a, b, c, d) . \quad (3.18)$$

Stationary values of W are then sought relative to variations in a, b, c and d. The integration with respect to x_1 and x_2 in eq. (3.5) is rather involved and results in a lengthy expression for W. However, the first variation of W with respect to a, b, c, and d results in an expression of the form

$$\delta W = f_1 \delta a + f_2 \delta b + f_3 \delta c + f_4 \delta d , \quad (3.19)$$

where

$$f_i = f_i(A_{ij}, B_{ij}, D_{ij}, N_1^T, N_2^T, M_1^T, M_2^T, L_1, L_2, a, b, c, d) , \quad i = 1, 4 .$$

For equilibrium

$$f_i = 0 , \quad i = 1, 4 . \quad (3.20)$$

Eqs. (3.20) constitute four algebraic equations for a, b, c, and d. The equations are nonlinear in a and b and linear in c and d. The equations are

$$\begin{aligned} f_1(a, b, c, d) = & -C_1 cb + C_2 ab^2 + 2C_3 ab - B_{11} c \\ & + D_{11} a - C_4 cb + 2C_5 ab^2 - C_6 db \\ & + D_{12} b - C_7 db + C_8 ab^2 + C_9 b^2 \\ & + (L_2^2/48) N_1^T b + M_1^T + (L_1^2/48) N_2^T b = 0 , \end{aligned} \quad (3.21a)$$

$$\begin{aligned} f_2(a, b, c, d) = & -C_1 ac + C_2 a^2 b + C_3 a^2 - C_4 ac + 2C_5 a^2 b + D_{12} a \\ & - C_6 da - C_7 da + C_8 a^2 b + 2C_9 ab - B_{22} d \\ & + D_{22} b + (L_2^2/48) N_1^T a + (L_1^2/48) N_2^T a + M_2^T = 0 , \end{aligned} \quad (3.21b)$$

$$f_3(a, b, c, d) = A_{11} c - C_1 ab - B_{11} a + A_{12} d - C_4 ab - N_1^T = 0 , \quad (3.21c)$$

$$f_4(a, b, c, d) = A_{12} c - C_6 ab - B_{22} b + A_{22} d - C_7 ab - N_2^T = 0 . \quad (3.21d)$$

In these equations

$$\begin{aligned} C_1 &= A_{11} L_2^2/48 , & C_2 &= A_{11} L_2^4/1280 , \\ C_3 &= B_{11} L_2^2/48 , & C_4 &= A_{12} L_1^2/48 , \\ C_5 &= A_{12} L_1^2 L_2^2/2304 , & C_6 &= A_{12} L_2^2/48 , \\ C_7 &= A_{22} L_1^2/48 , & C_8 &= A_{22} L_1^4/1280 , \\ C_9 &= B_{22} L_1^2/48 . \end{aligned} \quad (3.22)$$

It should be mentioned that when $L_1 = L_2 = 0$, the constants $C_1 - C_9$ are zero and eqs. (3.21) reduce to classical lamination theory, i.e., the geometrically linear case. Apparently, with the approach being used here, a laminate with zero sidelength is synonomus with classical lamination theory.

To obtain numerical results, eqs. (3.21) must be solved numerically. This can be done one of several ways. The four nonlinear algebraic equations can be solved using, for example, a Newton-type algorithm. Alternatively, it is possible to use the last two equations of eq. (3.21) and solve explicitly for c and d in terms of a and b. These expressions for c and d can be substituted into the first two equations to obtain two nonlinear equations for a and b. These two can be solved for by a and b by a Newton algorithm. As a final alternative, these two equations can be combined into a single equation for either a or b. HAMAMOTO and HYER (1985) used this approach. The alternative single equation for a is

$$(S^2U_1)a^5 + (S^2V_1)a^4 + (2SU_1U_2)a^3 + (STV_2 + 2SU_2V_1)a^2 + (SV_2^2 - T^2U_2 + U_1U_2^2)a + (U_2^2V_1 - TU_2V_2) = 0\,, \tag{3.23a}$$

with

$$b = -\frac{Ta + V_2}{Sa^2 + U_2}\,. \tag{3.23b}$$

Eqs. (3.23) use the following definitions:

$$\begin{aligned}
S &= \frac{A_{11}L_2^4 + A_{22}L_1^4}{2880}\,,\\
T &= D_{12} + \frac{A_{12}B_{11}B_{22}}{(A_{11}A_{22} - A_{12}^2)}\,,\\
U_1 &= D_{11} - \frac{A_{22}B_{11}^2}{(A_{11}A_{22} - A_{12}^2)}\,,\\
U_2 &= D_{22} - \frac{A_{11}B_{22}^2}{(A_{11}A_{22} - A_{12}^2)}\,,\\
V_1 &= M_1^T - \frac{B_{11}(A_{22}N_1^T - A_{12}N_2^T)}{(A_{11}A_{22} - A_{12}^2)}\,,\\
V_2 &= M_2^T - \frac{B_{22}(A_{11}N_2^T - A_{12}N_1^T)}{(A_{11}A_{22} - A_{12}^2)}\,.
\end{aligned} \tag{3.24}$$

With nonlinear algebraic equations, either eqs. (3.21) or eqs. (3.23), multiple roots and hence multiple configurations at a given ΔT can be expected. This correlates with the ability to predict multiple cylindrical shapes, as discussed in Section 2.

Given a specific laminate with a specific temperature change from cure, i.e., given A_{ij}, B_{ij}, D_{ij}, L_1, L_2, N_1^T, N_2^T, M_1^T, M_2^T, the out-of-plane deformations can be determined by solving for a and b. The inplane deformations c and d can also be determined, although here they are not of as much interest. As alluded to earlier, solutions to eqs. (3.21) are equilibrium solutions. At a given temperature one or more solutions may correspond to unstable equilibrium. Therefore the second variation of W must be examined for each solution. First, however, it is instructive to present numerical results regarding equilibrium shapes for specific laminates. The stability issues can thus be put into the context of specific shapes for specific laminates.

4. Numerical results

Numerical results for a specific laminate will illustrate clearly the important features of the relationship between laminate shape and the dimensions of the laminate, and between laminate shape and its temperature relative to cure. Recall in Section 2 that the only difference between the laminate in Fig. 1 and the laminate in Fig. 4 was the size of the laminate. This is the motivation for examining the influence of laminate size on its shape. On the other hand, raising and lowering the temperature of a laminate, relative to cure, is easily done and in fact is the method used by various investigators to determine the curing temperature of a laminate, PAGANO and HAHN (1977), HERAKOVICH et al. (1980). In addition, such an approach has been used to determine the influence of moisture and temperature of fiber-reinforced composite material, CROSSMAN et al. (1978), HYER and HAGAMAN (1979).

Fig. 7 illustrates the relationship between the size of a laminate and the shape of that laminate at room temperature (20°C). The results are from HAMAMATO and HYER (1985). The laminate considered is square, $L_1 = L_2 = L$, and the length of the side is on the horizontal axis. The values of a and b are the vertical axes of the two portions of the figure. The laminate is a $(0_4/90_4)_T$ laminate. Each lamina has the following properties

$$E_1 = 115\ \text{GPa}\,; \quad E_2 = 8\ \text{GPa}\,; \quad \nu_{12} = 0.28\,,$$

$$\alpha_1 = -0.106 \times 10^{-6}/°\text{C}\,; \quad \alpha_2 = 25.6 \times 10^{-6}/°\text{C}\,,$$

$$\text{lamina thickness} = 0.175\ \text{mm}\,; \quad \text{cure temperature} = 121°\text{C}\,.$$

For purposes of discussion, laminates made from laminae with these material properties will be referred to as type A laminates. The properties are representative of AS4/1908, a Hercules product, fabricated to 50% volume fraction fibers.

Immediately obvious from the figure are two factors. First, there is a symmetry to the solutions for the relation between a and b and sidelength. Second, there is the existence of three possible room-temperature equilibrium

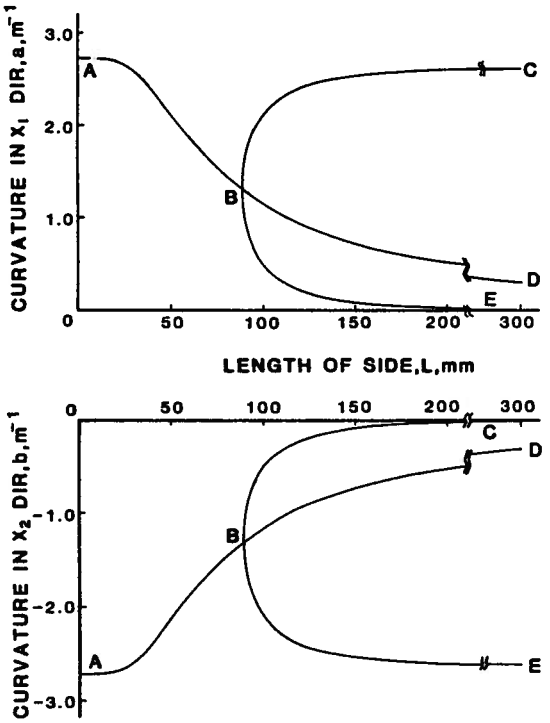

FIG. 7. Sidelength–curvature relation for square $(0_4/90_4)_T$ type A laminates at room temperature.

solutions if the laminate has a sidelength greater than some critical length. From the figure the critical length is 90 mm. For $L = 0$ there is only one solution. The solution is $b = -a$. This corresponds to a saddle shape. This, in fact, is the predicted shape if geometric nonlinearities are ignored in the analysis of shape prediction. This solution is denoted by point A on the figure. As the sidelength of the laminate increases from zero, say to 50 mm, the solutions are still single valued and the shape is still predicted to be a saddle. However, the saddle is one that is shallower than the linear prediction. As the sidelength increases even more, the saddle shape is still predicted to exist but it becomes even shallower. At some critical length the solution bifurcates. The bifurcation is denoted as point B on the figure. For sidelengths larger than this critical value, three equilibrium configurations are predicted to exist, each represented by a different solution branch on the figure. The branches are denoted as BC, BD and BE. Branch BD represents a continuation of the saddle shape. The other two solution branches represent a significant departure from a saddle shape. Ignoring for the moment the transition region near bifurcation (75 mm $\leq L \leq$ 150 mm), branch BC represents a laminate with a large positive curvature in the x_1 direction and little or no curvature in the x_2 direction. By contrast, branch BE represents a laminate with little or no

curvature in the x_1 direction and a large negative curvature in the x_2 direction. The shapes associated with these latter two branches can be considered cylindrical in nature and correspond with figs. 5(c) and 5(d). This variation in shape with laminate size corresponds well with the discussion in Section 2. For this 8 layer laminate, sidelengths greater than 90 mm will cause the laminate to cool to more than one equilibrium configuration. Obviously not all shapes occur simultaneously and some may correspond to unstable equilibrium configurations and will never be observed. This will be addressed later.

While the predictions of the dependence of laminate shape on size is interesting, the equations predict other interesting characteristics. Figs. 8–10 illustrate the dependence of type A laminate shape on temperature. In these figures the temperature–curvature relations of three laminates are shown, Fig. 8 illustrates the characteristics of a $125 \times 125\ mm^2$ laminate, Fig. 9 the characteristics of a $300 \times 300\ mm^2$, and Fig. 10 the characteristics of a $50 \times 50\ mm^2$ laminate. As before, there are two portions to each figure. Curvatures are on the vertical axes while the temperature of the laminate is on the horizontal axis. Room temperature (20°C) on the left end of the axis and the curing temperature (121°C) on the right end. The character of the shape can be traced with either increasing temperature of decreasing temperature. Only the latter situation will be discussed here.

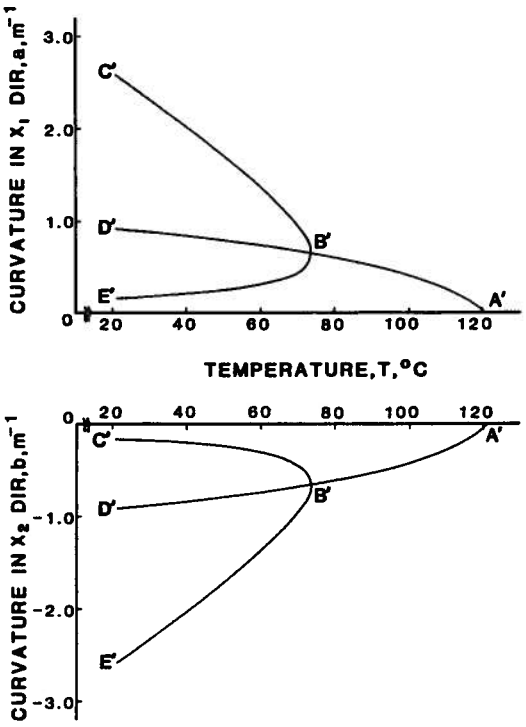

FIG. 8. Temperature–curvature relation for a 125 mm × 125 mm $(0_4/90_4)_T$ type A laminate.

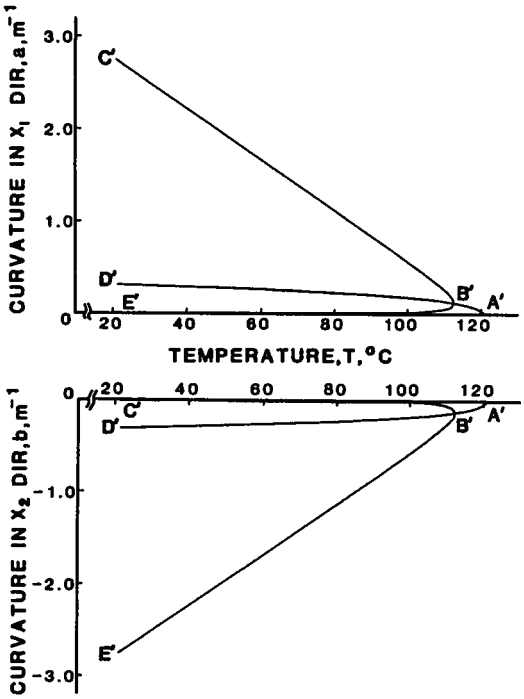

FIG. 9. Temperature–curvature relation for a 300 mm × 300 mm $(0_4/90_4)_T$ type A laminate.

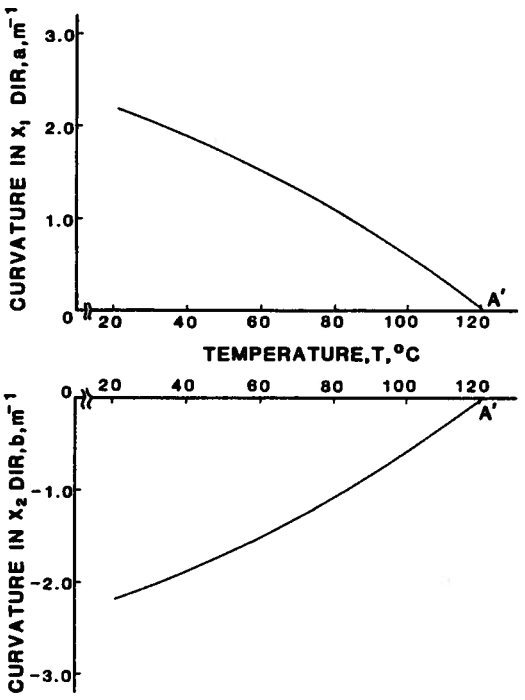

FIG. 10. Temperature–curvature relation for a 50 mm × 50 mm $(0_4/90_4)_T$ type A laminate.

Referring to Fig. 8, for the $125 \times 125\ mm^2$ laminate at the cure temperature, point A', the curvatures are zero. As the temperature decreases, curvatures develop. The curvatures are small but then are equal and opposite and so the laminate is saddle shaped. At roughly 77°C, point B', the solution bifurcates. The equilibrium solutions can follow one of three paths. These paths are denoted as B'C', B'D', and B'E'. If the laminate follows path B'C', the curvature in the x_1 direction continues to increase while the curvature in the x_2 direction decreases. Alternatively, if the laminate follows path B'E', the curvature in the x_1 direction decreases while the curvature in the x_2 direction increases, in magnitude. As a third possibility, if the laminate follows path B'D' as it cools, then it will remain saddle-shaped, the saddle becoming deeper and deeper as the temperature is lowered.

The temperature–curvature characteristics of the 300 mm × 300 mm laminate, Fig. 9, are similar to the temperature–curvature characteristics of the 125 mm × 125 mm laminate. For this larger laminate, however, the differences in the shapes represented by the different solutions branches are more distinct than they are for the $125 \times 125\ mm^2$ laminate. As the temperature is lowered from the stress-free temperature, equal and opposite curvatures develop. However, at less than 10°C below the stress-free temperature, the solutions bifurcate. If as the temperature is further reduced and the laminate follows path B'C', then the x_1-direction curvature continues to increase while the x_2-direction curvature virtually disappears. This corresponds to the cylindrical shape of Fig. 5(c). Alternatively, if the cooling path follows path B'E', then the x_2-direction curvature increases in magnitude and the x_1-direction curvature disappears. This corresponds to the cylindrical shape of Fig. 5(d). Path B'D' represents a laminate with equal and opposite curvatures, a saddle. For the $125 \times 125\ mm^2$ laminate, the shapes represented by branches B'C' and B'E' are not quite cylindrical. The tendency is there but the effect is not as pronounced as it is with the $300 \times 300\ mm^2$ laminate.

The small laminate, Fig. 10, shows a strikingly different temperature-curvature relation. For this laminate there is only one shape, a saddle, as the laminate cools from the cure temperature to room temperature. No bifurcation behavior occurs. In fact, the temperature–curvature relation is almost linear.

It should be mentioned that based on the description of the curing process earlier, the cooldown from cure occurs while the laminate is constrained between the caul plates. Therefore, the behavior shown in Figs. 8–10 does not occur. However, if after the laminate is removed from the caul plates it is heated to the cure temperature again and then cooled, the scenarios described in Figs. 8–10 are applicable.

With the numerical results for the $(0_4/90_4)_T$ laminate in hand, it is interesting to examine limiting value of a and b for large and small laminates. For a $(0_4/90_4)_T$ laminate $A_{22} = A_{11}$, $D_{22} = D_{11}$, $B_{22} = -B_{11}$. From eqs. (3.6), $N_2^T = N_1^T$, and $M_2^T = -M_1^T$. As a result, from eqs. (3.24), $U_2 = U_1$ and $V_2 = -V_1$. Eq. (3.23) provides the limiting information. For small laminates $L_1 \to 0$ and $L_2 \to 0$ and S of eq. (3.24) is zero. Eq. (3.23) gives

$$a = \left(\frac{24}{h}\,\frac{(Q_{11}Q_{22} - Q_{12}^2)(\alpha_1 - \alpha_2)\Delta T}{Q_{11}^2 + 14Q_{11}Q_{22} + Q_{22}^2 - 16Q_{12}^2}\right) \tag{4.1a}$$

and

$$b = -a\,. \tag{4.1b}$$

For large laminates $L_1 \to \infty$ and $L_2 \to \infty$. The first two terms in eq. (3.23) dominate and so

$$a = -\frac{U_1}{V_1} = \left(\frac{24}{h}\,\frac{(Q_{11}Q_{22} - Q_{12}^2)(\alpha_1 - \alpha_2)\Delta T}{Q_{11}^2 + 14Q_{11}Q_{22} + Q_{22}^2 - 16Q_{12}^2}\right)\left(\frac{Q_{11} + Q_{22} - 2Q_{12}}{Q_{11} + Q_{12}}\right) \tag{4.2a}$$

and

$$b = 0\,. \tag{4.2b}$$

The first bracketed term in eq. (4.2a) is the linear solution of eq. (4.1a) and the second bracketed term is slightly larger than unity for any material. Therefore, the large-laminate limit for the nonzero curvature is asymptotic to a value slightly larger than the linear prediction. The other curvature for the large laminate is zero.

At this point it is tempting to examine the effects of other parameters, such as laminate material properties, laminate thickness, or laminate stacking sequence, on the predicted shape or shapes. However, the information presented in the previous figures is not really complete until the stability of the predicted shapes is examined. This will be done and then the effects of the other parameters on the shapes and the stability of the shapes will then be examined.

5. Stability considerations

For any particular solution to the four algebraic equations, eqs. (3.21), to correspond to stable equilibrium, the total potential energy must be a minimum for the particular solution. If the total potential energy is not a minimum, the equilibrium condition is not stable and that particular equilibrium configuration will not be physically realized. For this discretized system the stability of the equilibrium configurations for the laminate is determined by examining the following determinant of partial derivatives of the four functions f_i, $i = 1, 4$, given in eqs. (3.21):

$$\begin{bmatrix} \frac{\partial f_1}{\partial a} & \frac{\partial f_1}{\partial b} & \frac{\partial f_1}{\partial c} & \frac{\partial f_1}{\partial d} \\ \frac{\partial f_2}{\partial a} & \frac{\partial f_2}{\partial b} & \frac{\partial f_2}{\partial c} & \frac{\partial f_2}{\partial d} \\ \frac{\partial f_3}{\partial a} & \frac{\partial f_3}{\partial b} & \frac{\partial f_3}{\partial c} & \frac{\partial f_3}{\partial d} \\ \frac{\partial f_4}{\partial a} & \frac{\partial f_4}{\partial b} & \frac{\partial f_4}{\partial c} & \frac{\partial f_4}{\partial d} \end{bmatrix}.$$

SIMITSES (1976) discusses this. A particular equilibrium configuration of a laminate with specific material properties, stacking sequence, and sidelength, and at a specific temperature is stable if and only if the matrix is positive definite. (For the cases studied here, the determinant of the matrix was not zero.) If the matrix is not positive definite, then the equilibrium configuration is not stable. Each point on each branch of the previous figures must be checked.

Using this scheme it was found that for the $(0_4/90_4)_T$ laminates in Figs. 7–10, any equilibrium configuration corresponding to a saddle shape is unstable if cylindrical equilibrium configurations can exist under the same conditions. If the saddle shape is the only shape that is predicted to exist, then it is stable. All cylindrical configurations in the figures are stable. Therefore, in Fig. 7, all the saddle configurations of branch AB are stable and will be observed at room-temperature. On the other hand, none of the saddle configurations on Branch BD are stable. For laminates with sidelengths greater than 90 mm, a saddle configuration will never be observed. Either of the two cylindrical configurations will be observed. On Figs. 8 and 9, as the flat laminate is cooled from the curing temperature alone path A′B′, a stable saddle configuration will develop. As the laminate is cooled below the bifurcation point, point B′, the saddle will cease to exist because it is unstable. The laminate will deform into either the cylinder represented by path B′C′, or the cylinder represented by path B′E′. By contrast, when the smaller laminate is cooled, Fig. 10, it deforms into a stable saddle and remains that way for all temperatures below the cure temperature.

From the information presented in the analysis it is not possible to determine which of the two cylindrical configurations of Figs. 7, 8, and 9 will be observed. Since both cylindrical configurations are stable, they correspond to total potential energy minimums. These are local minimums in the sense that they were determined by examining variations of the configurations, i.e., variational displacements are by definition small. Therefore either configuration is likely. In reality, small imperfections in the laminate or small variations from a spatially uniform temperature will cause the laminate to favor one cylindrical configuration or the other.

With all the components available to determine the shapes of unsymmetric laminates and to determine whether or not the shapes will ever be observed, the effects of material properties, stacking sequence, and other variables are now examined.

6. Other numerical results

6.1. *Effect of material properties*

The effect of material properties on the shape response can be examined by considering laminates fabricated from lamina with the following material properties:

$$E_1 = 181\ \text{GPa}\ ;\quad E_2 = 10.3\ \text{GPa}\ ;\quad \nu_{12} = 0.28\ ,$$

$$\alpha_1 = -0.106 \times 10^{-6}/°\text{C}\ ;\quad \alpha_2 = 25.8 \times 10^{-6}/°\text{C}\ ,$$

lamina thickness = 0.100 mm ; cure temperature = 177°C .

Compared with the first material examined, this material has a higher cure temperature and is stiffer in both the fiber direction and perpendicular to the fibers. It is expected that this will influence the temperature–curvature and curvature–sidelength relations. Laminates made from lamina with these material properties will be referred to as type B laminates. The properties are representative of a material with T300 fibers and 5208 resin, with 60% volume fraction fibers, HYER (1981b).

Fig. 11 illustrates the sidelength–curvature relation at room-temperature for a $(0_4/90_4)_T$ laminate fabricated from this second material. Only the x_1-direction curvature is shown. The x_2-direction curve has the mirror image symmetry of Fig. 7. Compared to Fig. 7, the analogous figure for type A material, there are not many differences. The main differences are the magnitude of the large-laminate curvature, and the length corresponding to the bifurcation point. Compared with the type A material, the magnitude of the curvature, for a given sidelength, is slightly larger. On the other hand, the bifurcation sidelength is slightly smaller. A stability analysis indicates identical stability characteristics.

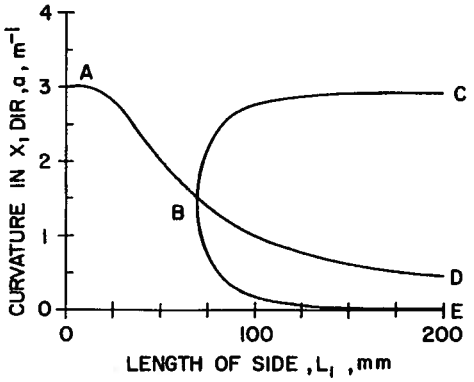

FIG. 11. Sidelength–curvature relation for square $(0_4/90_4)_T$ type B laminates at room temperature.

6.2. *Effect of laminate thickness*

Fig. 12 illustrates the shape characteristics of a $(0_2/90_2)_T$ laminate. The material considered is type B, HYER (1981b). Except for thickness, the laminate of Fig. 11 and the laminate of Fig. 12 are identical. To determine the effect of laminate thickness, this figure can be compared directly with Fig. 11.

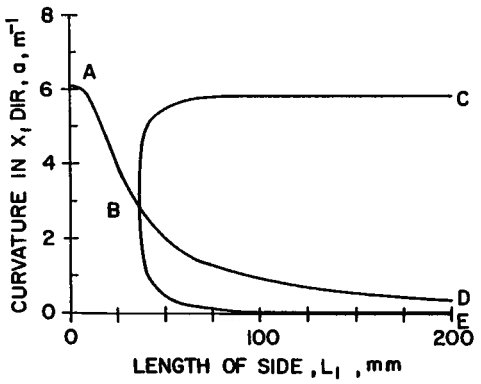

FIG. 12. Sidelength–curvature relation for square $(0_2/90_2)_T$ type B laminates at room temperature.

Two differences between the cases are immediately obvious. First the magnitude of the curvatures differ by a factor of two, the thinner laminate having larger curvatures. A 150 mm × 150 mm $(0_2/90_2)_T$ laminate, for example, has twice the out-of-plane deflection as a 150 mm × 150 mm^2 $(0_4/90_4)_T$ laminate. The second difference is the location of the bifurcation point. Bifurcation of the solutions for the $(0_2/90_2)_T$ laminate occurs when the sidelength reaches 36 mm. The thicker laminate can be twice as large before the saddle-shape configuration disappears and the laminate becomes cylindrical. If the governing equations are nondimensionalized, it can be shown that the laminates of the family $(0_n/90_n)_T$, $n = 1, 2, \ldots$, the transition from saddle to cylinder occurs at the value of L/h of 72.

6.3. *Effect of laminate aspect ratio*

So far the laminates discussed have all been square. The sidelength in the x_1 direction has been the same as the sidelength in the x_2 direction. Figs. 13–16 show the effect of two other aspect ratios on laminate shape, HYER (1981c). Here aspect ratio will be defined as the sidelength in the x_2 direction divided by the sidelength in the x_1 direction, L_2/L_1. Because of the symmetry of the a and b variation with sidelength, only the variation of a with sidelength is illustrated.

In addition, the sidelength in the x_1 direction, L_1, is used as the length variable.

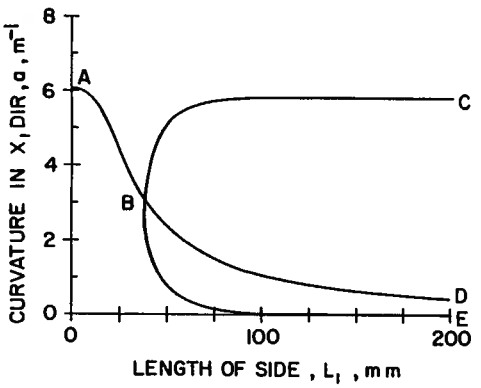

FIG. 13. Sidelength–curvature relation for $(0_2/90_2)_T$ type B laminates at room temperature, aspect ratio $L_2/L_1 = 0.25$.

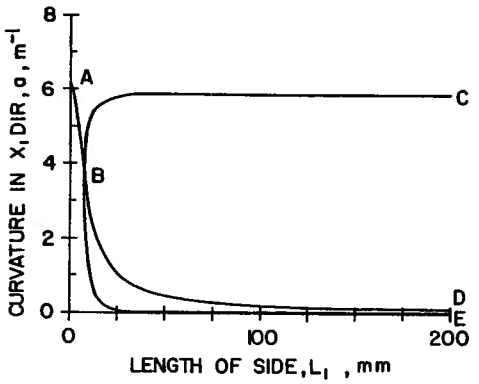

FIG. 14. Sidelength–curvature relation for $(0_2/90_2)_T$ type B laminates at room temperature, aspect ratio $L_2/L_1 = 4$.

Fig. 13 shows the relationship between the curvature in the x_1 direction and L_1 for a rectangular $(0_2/90_2)_T$ type B laminate with an aspect ratio of 0.25. Qualitatively the characteristics are similar to previous cases presented. There is a length range for which the solution is single-valued and a length range for which there are three solutions. Roughly, multiple solutions occur when L_1 is greater than 36 mm. All solution branches except the saddle branch BD represent stable equilibrium configurations. Except for the region around the bifurcation point, the sidelength–curvature relation for this laminate is very similar to the relation for a square $(0_2/90_2)_T$ laminate (Fig. 12).

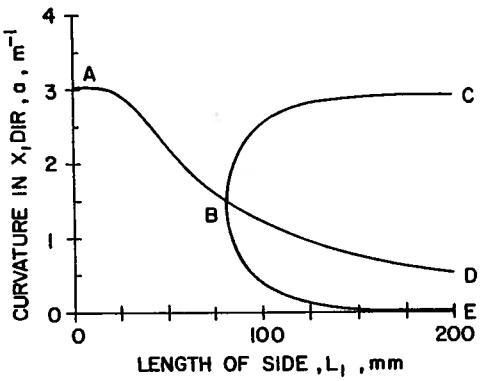

FIG. 15. Sidelength–curvature relation for $(0_4/90_4)_T$ type B laminates at room temperature, aspect ratio $L_2/L_1 = 0.25$.

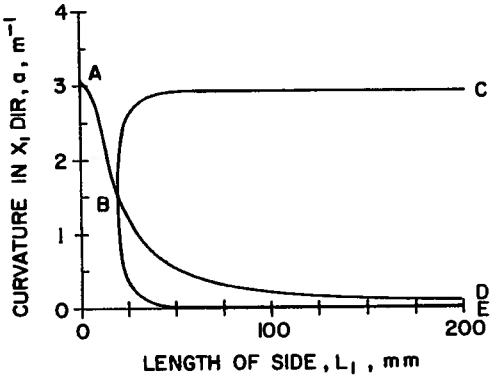

FIG. 16. Sidelength–curvature relation for $(0_4/90_4)_T$ type B laminates at room temperature, aspect ratio $L_2/L_1 = 4$.

Markedly different behavior is observed if the aspect ratio is changed so that the laminate is four times longer in the x_2 direction than in the x_1 direction. Fig. 14 shows the behavior of such a laminate. The figure indicates that the length range of single-valued solutions is much less for this laminate. Multiple solutions occur when L_1 exceeds 9 mm. The saddle configuration represented by branch BD is unstable and the curvature for large laminates, i.e., $L_1 >$ 25 mm, is the same as for square laminates or for laminates with an aspect ratio of 0.25.

Figs. 15 and 16 show the sidelength–curvature relation for the thicker $(0_4/90_4)_T$ type B laminates with aspect ratios of 0.25 and 4, respectively. Fig. 11 illustrated the behavior of square laminates of this thickness. By comparing Figs. 11, 15 and 16 it is clear that the square laminate and the laminate with an

aspect ratio of 0.25 behave similarly. However, the laminate with an aspect ratio of 4 has larger sidelength range over which the multiple solutions occur.

From the results illustrated, it appears that for rectangular laminates, the location of the bifurcation point depends on the length of the longer side. In all cases shown, for the type B laminates, when the length of the longer side divided by the laminate's total thickness exceeds 72, multiple solutions occurred. Similar studies have not been conducted for the type A laminate but similar behavior is expected. The numerical value of the critical length-to-thickness ratio, however, is expected to be material-dependent.

6.4. *Effect of stacking sequence*

It is interesting to consider other stacking arrangements and study their shapes, HYER (1982). Here the discussion will be limited to square laminates. If just four-layer cross-ply laminates are considered, there are only four unique stacking arrangements. All other arrangements can be obtained from the four by a simple rotation of the laminate in its plane or by turning the laminate upside down. The four unique arrangements are: the $(0/0/90/90)_T$ previously discussed in Fig. 12; $(0/90/0/90)_T$; $(0/0/0/90)_T$; and $(0/90/0/0)_T$. The equilibrium configurations of these latter three laminates now will be discussed. For the discussion material properties of a type B laminate will be used.

Fig. 17 shows the sidelength–curvature relation for the $(0/90/0/90)_T$ laminate. The equilibrium configurations of this laminate are quite similar to the configurations of the $(0_2/90_2)_T$ of Fig. 12. However, some interesting differences can be observed. First, the out-of-plane deflections of the $(0/90/0/90)_T$ laminate are not as large as the deflections of the $(0_2/90_2)_T$ case. This is because the asymmetry in the laminate material properties for the $(0/90/0/90)_T$ is not as severe as the asymmetry in the $(0_2/90_2)_T$ case. Second, and directly related to the degree of asymmetry, this laminate will exhibit saddle-shape equilibrium configurations for sidelengths up to 87 mm. This is opposed to the 37 mm sidelength limit for the $(0_2/90_2)_T$ laminate. The level of asymmetry in the material properties of the laminate is reflected in the magnitude of the terms in the B_{ij} matrix and the magnitude of the effective thermal moments.

Figs. 18 and 19 show the sidelength–curvature relation for a $(0/0/0/90)_T$ and a $(0/0/90/0)_T$ laminate, respectively. These relationships are unlike any discussed so far. The most striking difference between the relationship for these laminates and the relationship for the other laminates discussed is the lack of a coalescence of the solution branches. Whereas the branching of solutions from a common point is referred to as bifurcation behavior, the disjoint behavior of the sidelength–curvature relationship for these laminates is referred to as limit point behavior. For unsymmetric laminates bifurcation behavior is generally associated with perfect or mathematically ideal conditions. Limit point behavior is associated with a lack of ideal conditions. The lack of idealism is

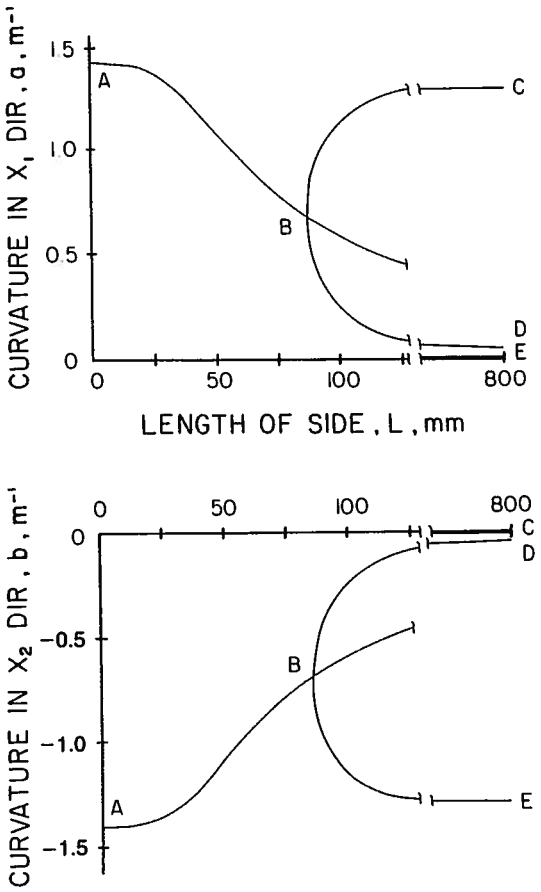

FIG. 17. Sidelength–curvature relation for $(0/90/0/90)_T$ type B laminates at room temperature.

reflected in the A, B and D matrices as well as in the effective thermal loads. For the ideal situation, $A_{22} = A_{11}$, $B_{22} = -B_{11}$, $D_{22} = D_{11}$, $N_1^T = N_2^T$, and $M_2^T = -M_1^T$. If one or more of these equalities is violated, bifurcation behavior will not occur.

Referring to Fig. 18, for a $(0/0/0/90)_T$ laminate of zero sidelength, i.e., the solution when geometric nonlinearities are ignored, the room-temperature shape is predicted to be a saddle. However, the saddle is not a perfect saddle, rather, the curvature in the x_1 direction is much smaller than the curvature in the x_2 direction. As the sidelength increases from zero, the smaller of the two curvatures begins to decrease rapidly. At a sidelength of 100 mm, the minor curvature has disappeared and the laminate is cylindrical, all the curvature being in the x_2 direction. As the sidelength increases to about 200 mm, multiple equilibrium configurations occur. One solution branch is the continuation of cylindrical branch AE. The other solution branches represent different equilibrium configurations. (Note that on the figure the curvatures in the x_2 direction

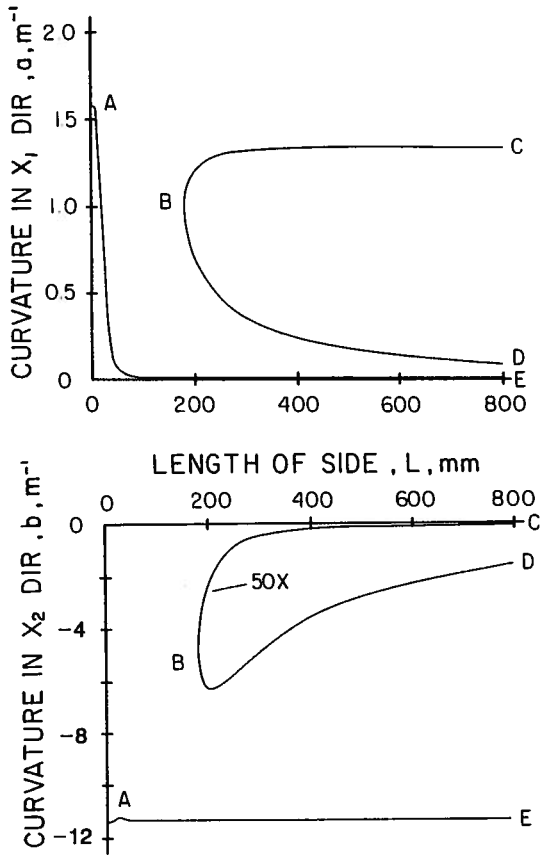

FIG. 18. Sidelength–curvature relation for square $(0/0/0/90)_T$ type B laminates at room temperature.

have been multiplied by 50 before plotting them.) At 400 mm, for example, branch BC represents a cylindrical configuration with no curvature in the x_2 direction. The curvature in the x_1 direction is roughly equal to the linear solution prediction. Branch BD represents a saddle configuration. Both curvatures are small but they are of opposite sign. It would be impossible, however, to detect the curvature in the x_2 direction for this particular case. Which of the three equilibrium will actually be observed is determined by examining stability.

A stability analysis predicts interesting results. Branch AE corresponds to stable equilibrium configurations. Branch BC also represents stable shapes. Branch BD corresponds to unstable configurations. Unlike the other laminates discussed, the existence of a unique and stable cylindrical shape is predicted. A 100 mm × 100 mm laminate, for example, will have a cylindrical shape and it cannot be forced into another cylindrical shape. Larger laminates, say

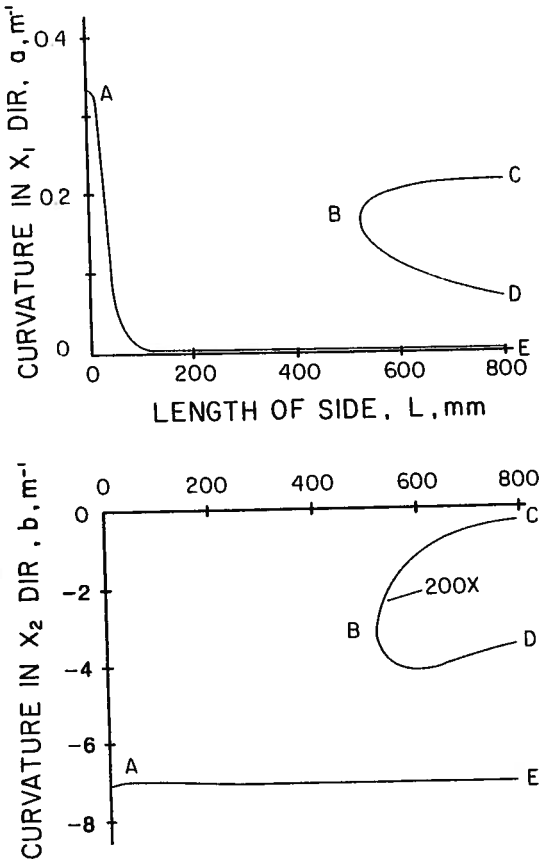

FIG. 19. Sidelength–curvature relation for square $(0/0/90/0)_T$ type B laminates at room temperature.

600 mm × 600 mm, can be made to have either of two cylindrical shapes. One of the shapes has the same curvature characteristics a 100 mm × 100 mm laminate would, i.e., branch AE. The other cylindrical shape would correspond to branch BC. The saddle configuration would never be observed for a 600 mm × 600 mm laminate.

The sidelength–curvature characteristics of a $(0/0/90/0)_T$ type B laminate, Fig. 19, are much like those of the $(0/0/0/90)_T$ laminate. Limit point behavior, instead of bifurcation behavior, is predicted. Compared to a $(0/0/0/90)_T$ laminate, the curvatures are smaller and the laminate can be made larger before multivalues solutions occur. Again, this can be attributed to the less severe degree of asymmetry for the $(0/0/90/0)_T$ can as compared to the $(0/0/0/90)_T$ case. This is clear if one considers that a $(0/0/0/0)_T$ has no asymmetry. If the lamina furthest from the laminate's geometric midplane is given a 90° orientation, the asymmetry in laminate material properties and

thermal loads is greater than if the lamina closest to the geometric midplane is given a 90° orientation.

It should be noted that in the region of the sidelength–curvature relation where the smaller curvature is rapidly disappearing, the nonzero curvature (branch AE in the b portion of each figure) has a slight perturbation. The nonzero curvature decreases in magnitude very slightly as the length increases and then the curvature increases in magnitude again. This behavior would probably not be detected in an actual laminate.

7. Closure

This chapter has discussed an interesting phenomenon in the mechanics of composite materials. It has not been widely discussed before but the results explain behavior often observed in composite laminates. Though only simple laminates were considered, the same basic predictions are expected to occur for more complicated laminates.

Acknowledgements

The work discussed here was supported by the NASA-Virginia Tech Composites Program, Cooperative Agreements NCCl-15 and NAG-1-343, and Grant 81-0195 with the United States Air Force Office of Scientific Research, and Contract F49620-79-C-0038 with the United States Air Force Office of Scientific Research.

References

AGARWAL, B.D. and L.J. BROUTMAN (1980), *Analysis and Performance of Fiber Composites* (John Wiley and Sons, New York) pp. 145–156.

CROSSMAN, F.W., R.E. MAURI and W.J. WARREN (1978), Moisture-altered viscoelastic response of graphite–epoxy composites, in: J.R. Vinson, ed., *Advanced Composite Materials-Environmental Effects* (STP-658, American Society for Testing and Materials, Philadelphia, PA) pp. 205–220.

HAMAMOTO, A. and M.W. HYER (1987), *Int. J. of Solids and Structures* **23**, 919–935.

HERAKOVICH, C.T., J.G. DAVIS, Jr and J.S. MILLS (1980), Thermal microcracking in celion 6000/PMR-15 graphite-polyimide, in: D.P.H. HASSELMAN and R.A. HELLER, eds., *Thermal Stresses in Severe Environment* (Plenum Publishing Press, New York) pp. 649–665.

HYER, M.W. (1981a), *J. Comp. Mater.* **15**, 175–194.

HYER, M.W. (1981b), *J. Comp. Mater.* **15**, 296–340.

HYER, M.W. (1981c), An inherent instability in fiber-reinforced composite laminates, in: S.S. WANG and W.J. RENTON, eds., *Advances in Aerospace Structures and Materials-AD-01* (American Society of Mechanical Engineers, New York) pp. 239–246.

HYER, M.W. (1982), *J. Comp. Mater.* **16**, 318–340.

HYER, M.W. and J.A. HAGAMAN (1979), The effects of thermal cycling on the thermal deformations of graphite-polyimide, *Proc. Spring Meeting of the Society of Experimental Stress Analysis*, San Francisco, CA, paper no. R79-114 (Society of Experimental Mechanics, Brookfield Center, CT).

JONES, R.M. (1975), *Mechanics of Composite Materials* (McGraw-Hill, New York) pp. 147–156.

PAGANO, N.J. and H.T. HAHN (1977), Evaluations of composite curing stresses, in: J.G. DAVIS JR, ed., *Composite Materials: Testing and Design, 4th Conf.* (STP 617, American Society for Testing and Materials, Philadelphia, PA) pp. 317–329.

SIMITSES, G.J. (1976), *An Introduction to the Elastic Stability of Structures* (Prentice-Hall, Inc., Englewood Cliffs, NJ) pp. 8–14.

TSAI, S.W. and H.T. HAHN (1980), *Introduction to Composite Materials* (Technomic Publishing Co., Westport, CT) pp. 217–276.